18

Plant Biomass Characterization: Application of Solution- and Solid-state NMR Spectroscopy

Yunqiao Pu[1,3], Bassem Hallac[2,3] and Arthur J. Ragauskas[1,2,3]

[1] *Georgia Institute of Technology, Atlanta, USA*

[2] *School of Chemistry and Biochemistry, Georgia Institute of Technology, Atlanta, USA*

[3] *BioEnergy Science Center, Oak Ridge, USA*

18.1 Introduction

Releasing fermentable sugars from lignocellulosic materials remains challenging due to resistance of plants to breakdown. A pretreatment stage is required to reduce this recalcitrance, which is considered to be the most intensive operating cost component of cellulosic ethanol production. There are different features that make plant biomass resistant to chemical and biological degradation, such as lignin content/structure, lignin-carbohydrate complexes (LCCs), hemicellulose content, as well as cellulose ultrastructure and degree of polymerization (DP). Research on this subject is therefore focused on understanding the effects of pretreatment technologies on the reduction of biomass recalcitrance as well as on fundamental structural characteristics of biomass that impact pretreatment and subsequent enzymatic hydrolysis. Improving our fundamental knowledge of pretreatment technologies will lead to significant advances in the field of sustainable low-cost cellulosic biofuels production [1].

Nuclear magnetic resonance (NMR) spectroscopy is a powerful tool for detailed structural elucidation of the major constitutes of plant biomass, lignin, hemicellulose, and cellulose [2–8]. Many of the structural details/characteristics of biopolymers (especially lignin) in native and transgenic plant biomass we know of today were revealed with NMR measurements, in addition to key information about lignin/hemicellulose synthesis in plants as well as plant genetic engineering [2,3]. This chapter focuses on the application of solution- and solid-state NMR spectroscopy techniques to characterize the structural features of cellulose

Aqueous Pretreatment of Plant Biomass for Biological and Chemical Conversion to Fuels and Chemicals, First Edition.
Edited by Charles E. Wyman.

and lignin during aqueous pretreatment of plant biomass for biological and chemical conversion to fuels and chemicals. Specifically, the most commonly employed solution-state NMR techniques including one-dimensional (1D) ^{1}H, ^{13}C, and ^{31}P NMR and two-dimensional (2D) heteronuclear single quantum coherence (HSQC) will be discussed for lignin structure characterization. Solid-state cross-polarization/magic angle spinning (CP/MAS) ^{13}C NMR will also be reviewed as the technique used for analysis of the crystallinity and ultrastructure of plant cellulose.

18.2 Plant Biomass Constituents

Plant biomass, including woody and herbaceous lignocellulosics, is a natural biocomposite primarily composed of three major biopolymers (i.e., cellulose, hemicellulose, and lignin), usually with minor amounts of inorganics and extractives. In a plant cell wall, these polymers typically interact with each other physically and chemically to form an intricate three-dimensional network structure. Plants have a complicated and dynamic cell wall which is generally composed of three anatomical regions, that is, middle lamella, the primary cell wall, and the secondary cell wall. The cell types and chemical compositions vary among different species as well as among various regions of the same plant.

The predominant polysaccharide in plant biomass is cellulose, which is a linear homopolymer of (1 → 4)-linked β-D-glucopyranosyl units with the degree of polymerization varying from 300 to *c.* 15 000 [9,10]. The hydroxyl groups on these glucopyranosyl units have a strong tendency to form intra- and intermolecular hydrogen bonds among the linear glucan chains, which stiffen the chains and can facilitate cellulose aggregations to form highly ordered or crystalline cellulose fibril structures. Most plant celluloses also contain varying degrees of amorphous domains that are more amenable to chemical and enzymatic attack.

After cellulose, the next major polysaccharide in plant biomass is hemicellulose. Hemicelluloses generally refer to a group of mixed heteroglycans of pentoses and hexanoses which link together in a plant with a DP of *c.* 70–200 and frequently have branching and substitution groups [11,12]. The major hemicelluloses in softwoods include glucomannans and arabinoglucuronoxylan, while in many hardwood and herbaceous plants the predominant hemicellulose is glucuronoxylan.

Compared to cellulose and hemicellulose, lignin does not have a distinct chemical structure. Lignin is an amorphous and irregular polyphenolic biopolymer that is synthesized by enzymatic dehydrogenative polymerization of phenylpropanoid monolignols. Three types of phenylpropane units are generally considered as basic building blocks for biosynthesis of protolignin: coniferyl, sinapyl, and *p*-coumaryl alcohol (Figure 18.1), which correspond to the guaiacyl (G), syringyl (S) and *p*-hydroxyphenyl (H) structures of lignin, respectively [13–15]. Softwood lignin contains predominantly guaiacyl and minor amounts of

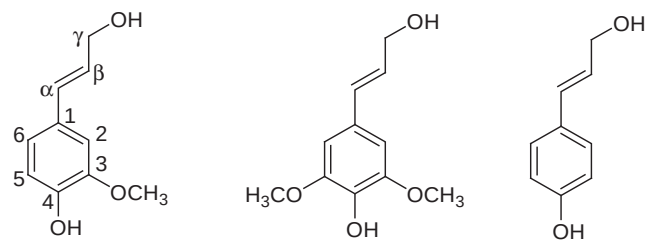

Figure 18.1 *Phenylpropanoid units involved in lignin biosynthesis [13].*

p-hydroxyphenyl units, while hardwood lignin is primarily composed of guaiacyl and syringyl units. Lignin in herbaceous plants generally contains all three types of monolignol units, with a core structure composed mainly of guaiacyl and syringyl units and incorporated peripheral groups such as *p*-hydroxycinnamic acid and ferulic acid units [14,15].

18.3 Solution-state NMR Characterization of Lignin

Lignin is considered as one of the most recalcitrant components in plant cell walls and protects plants against microbial and enzymatic deconstruction. Lignin is intimately associated with carbohydrate components in the cell walls of vascular plants, forming an amorphous network embedding microfibril cellulosic materials. The lignin macromolecule is primarily connected through carbon-carbon and carbon-oxygen ether bonds among the building blocks of phenylpropane monomers [13]. The structure of lignin is complex, irregular, and highly heterogeneous, with no regular extended repeating unit structures observed. Compared to other biopolymers, the structural determination of lignin is more challenging due to its complexity and the difficulty in isolation of a highly representative and structurally unchanged lignin sample from plant species. Although the exact structure of protolignin in a plant is still not fully understood, advances in spectroscopic methods (especially NMR techniques) and computational modeling have enabled scientists to elucidate the predominant structural features of lignin, such as inter-unit linkages and their relative abundances in plant biomass. Some common inter-unit linkages identified in lignin, such as β-O-4, α-O-4/β-5 (phenylcoumaran), β-β (pinoresinol), dibenzodioxocin, and 4-O-5, are presented in Figure 18.2. The relative proportions of such units are usually dependent on the biomass species as well as the processing methods employed [11,16]. The discovery of dibenzodioxocin in softwood lignins at a level of *c.* 10–15% in the early 1990s has initiated a flurry of research efforts that led to detection/identification of several new subunit structures such as spirodienone [17–21].

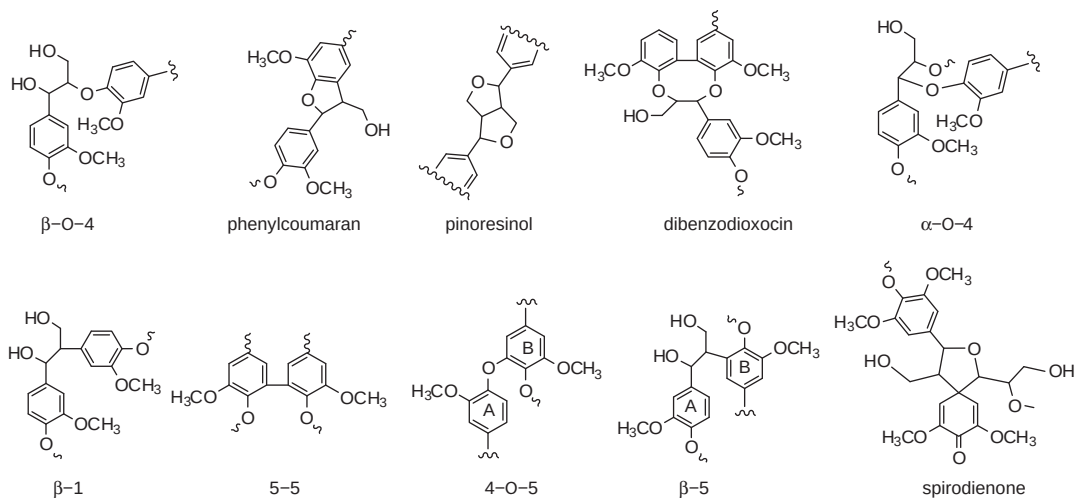

Figure 18.2 *Typical inter-unit linkages in plant lignins.*

18.3.1 Lignin Sample Preparation

No applicable method has yet been developed that can be regarded as ideal for the isolation of a highly representative native lignin with unaltered structures from plant biomass materials. To date, the most commonly used methods for lignin isolation are ball-milled lignin isolation developed by Bjorkman and cellulolytic enzyme lignin (CEL) preparation [22–24]. The Bjorkman method involves extensive milling of the plant materials followed by extraction with neutral solvents of dioxane-water at room temperature [22]; the resulting isolated material is usually referred to as milled wood lignin (MWL) when dealing with woody biomass. The milling is carried out either in a non-swelling medium such as toluene or in the dry state, usually under inert atmospheric gases such as nitrogen or argon in the milling jar. This method generally offers a low or moderate lignin yield (up to *c.* 25%), depending upon various plant species. Despite its low/moderate yield and possible structural alteration during milling, this methodology is widely accepted as a typical lignin isolation method, affording a lignin sample with minimal structural alteration and the closest native representation.

CEL preparation treats finely ground (i.e., ball-milled) plant powders with cellulolytic enzymes prior to solvent extraction to partially remove polysaccharides [23]. The enzymatically treated plant meal is then successively extracted with 96% and 50% aqueous dioxane, yielding two lignin fractions. Compared to the traditional Bjorkman procedure, the CEL procedure offers a significantly improved lignin yield (up to 55%) for various species, which is probably more representative of total lignin in a plant. However, this preparation usually suffers from higher carbohydrate contamination (*c.* 10–12% for a spruce wood compared to less than 5% in the Bjorkman procedure) of the lignin and is a more tedious and time-consuming process [24].

18.3.2 ^{1}H NMR Spectroscopy

^{1}H NMR spectroscopy is a valuable technique for characterization and classification of lignin structural features. Earlier work on the characterization of lignin by NMR mainly relied on ^{1}H NMR spectroscopy, and extensive databases of ^{1}H NMR chemical shifts were established for lignin model compounds and functional groups [6,8]. One advantage of ^{1}H NMR is that the ^{1}H nucleus is the most abundant among the nuclei that can be detected by NMR, thus giving a high signal to noise (S/N) ratio in a short experimental time (typically within several minutes). The drawback of ^{1}H NMR for lignin analysis is that it usually suffers from severe signal overlaps due to its short chemical shift ranges (i.e., δ *c.* 12–0 ppm) [8]. For ^{1}H NMR characterization of lignin, the samples can be examined either as acetate derivatives or underivatized forms. Acetylated lignin generally provides improved spectral resolution; however, the acetylation procedure may cause some unwanted chemical modifications to the sample. ^{1}H NMR of underivatized lignin is informative about some key lignin functionalities. For example, Li and Lundquist showed that ^{1}H NMR can be employed to quantify carboxylic acids, aromatic hydrogens, and formyl and methoxyl groups in an underivatized lignin [25]. Table 18.1 lists assignments and chemical shifts of typical structural features of acetylated spruce MWL in a ^{1}H NMR spectrum [8]. Figure 18.3 provides an example of ^{1}H NMR spectrum of underivatized MWL isolated from a poplar biomass which was recorded in a Bruker 400-MHz NMR instrument.

18.3.3 ^{13}C NMR Spectroscopy

^{13}C NMR spectroscopy is one of the most reliable and frequently used techniques for lignin characterization, providing comprehensive information about the structures of all carbons in lignin molecules [5]. It benefits from a broader spectral window (i.e., δ *c.* 240–0 ppm) in comparison to ^{1}H NMR, with better resolution and less overlap of signals. A routine qualitative ^{13}C NMR spectrum of lignin is generally recorded

Table 18.1 *Typical signals assignment and chemical shifts in the ^{1}H NMR spectrum of acetylated spruce lignin using deuterated chloroform as solvent [8].*

δ (ppm)	Assignment
1.26	Hydrocarbon contaminant
2.01	Aliphatic acetate
2.28	Aromatic acetate
2.62	Benzylic protons in β-β structures
3.81	Protons in methoxyl groups
4.27	H_γ in several structures
4.39	H_γ in, primarily, β-O-4 structures and β-5 structures
4.65	H_β in β-O-4 structures
4.80	Inflection possibly due to H_α in pinoresinol units and H_β in noncyclic benzyl aryl ethers
5.49	H_α in β-5 structures
6.06	H_α in β-O-4 structures (H_α in β-1 structures)
6.93	Aromatic protons (certain vinyl protons)
7.41	Aromatic protons in benzaldehyde units and vinyl protons on the carbon atoms adjacent to aromatic rings in cinnamaldehyde units
7.53	Aromatic protons in benzaldehyde units
9.64	Formyl protons in cinnamaldehyde units
9.84	Formyl protons in benzaldehyde units

with a pulse angle in the range 30–60°, a pulse delay of *c.* 0.5–2 s, and the transient number of about 10 000–20 000. Quantitative information about specific functional groups and structures present in lignin can be also estimated when the ^{13}C NMR spectrum is recorded under quantitative requirement conditions, although the recording of spectra is time consuming. In general, a quantitative ^{13}C NMR spectrum with a satisfactory signal-to-noise ratio is obtained at *c.* 50 °C using a 90° pulse, a pulse delay of about 12 s, an inversed gated decoupling pulse sequence, and thousands of transient acquisition numbers. The total experiment time is much longer than typical ^{1}H NMR, usually being up to 24–36 h.

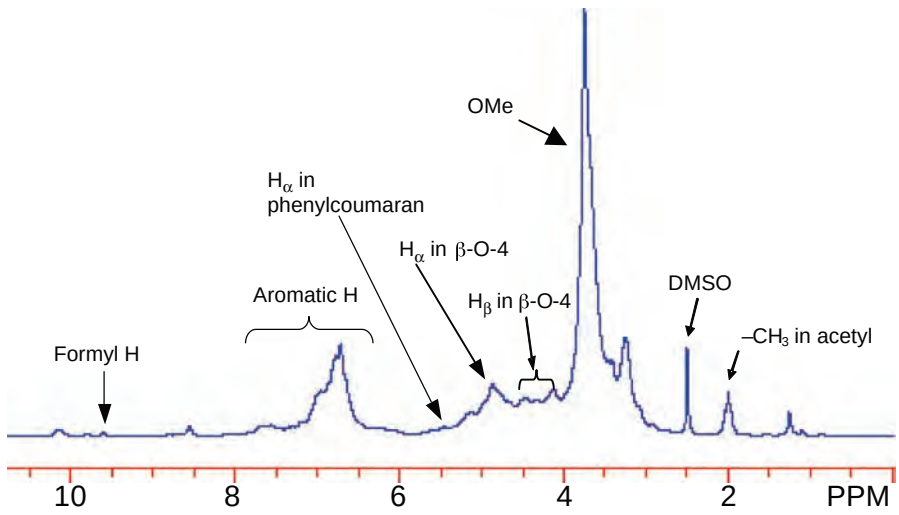

Figure 18.3 *An example of ^{1}H NMR spectrum of a poplar mill-wood lignin using DMSO as solvent.*

Table 18.2 *Typical chemical shifts and signal assignments for a spruce milled wood lignin (MWL) in a ^{13}C NMR spectrum [5,26,27]..*

δ (ppm)	Assignment
193.4	C=O in Ar—CH=CH—CHO; C=O in Ar—CO—CH(—OAr)—C—
191.6	C=O in Ar—CHO
169.4	Ester C=O in R′—O—CO—CH_3
166.2	C=O in Ar—COOH; Ester C=O in Ar—CO—OR
156.4	C-4 in H-units
152.9	C-3/C-3′ in etherified 5-5 units; C-α in Ar—CH=CH—CHO units
152.1	C-3/C-5 in etherified S units and B ring of 4-O-5 units[a]
151.3	C-4 in etherified G units with α-C=O
149.4	C-3 in etherified G units
149.1	C-3 in etherified G type β-O-4 units
146.8	C-4 in etherified G units
146.6	C-3 in non-etherified G units (β-O-4 type)
145.8	C-4 in non-etherified G units
145.0	C-4/C-4′ of etherified 5-5 units
143.3	C-4 in ring B of β-5 units[a]; C-4/C-4′ of non-etherified 5-5 units
134.6	C-1 in etherified G units
132.4	C-5/C-5′ in etherified 5-5 units
131.1	C-1 in non-etherified 5-5 units
129.3	C-β in Ar—CH=CH—CHO
128.0	C-α and C-β in Ar-CH=CH—CH_2OH
125.9	C-5/C-5′ in non-etherified 5-5 units
122.6	C-1 and C-6 in Ar—CO—C—C units
119.9	C-6 in G units
118.4	C-6 in G units
115.1	C-5 in G units
114.7	C-5 in G units
111.1	C-2 in G units
110.4	C-2 in G units
86.6	C-α in G type β-5 units
84.6	C-β in G type β-O-4 units (threo)
83.8	C-β in G type β-O-4 units (erythro)
71.8	C-α in G type β-O-4 units (erythro)
71.2	C-α in G type β-O-4 units (threo); C-γ in G type β-β
63.2	C-γ in G type β-O-4 units with α-C=O
62.8	C-γ in G type β-5, β-1 units
60.2	C-γ in G type β-O-4 units
55.6	C in Ar—OCH_3
53.9	C-β in β-β units
53.4	C-β in β-5 units
40-15	CH_3 and CH_2 in saturated aliphatic chain

[a] see Figure 18.2 for structures; Ar: aromatic.

Quantitative data on lignin structural features is usually reported on the basis of the phenylpropane by calculating the ratio of the integral value of a given carbon signal to one-sixth the integral of the aromatic carbons whose signals are located in the range *c.* 102–162 ppm [5]. Corrections need to be made if a sample contains structural features with vinyl carbons that appear in this region. Figure 18.4 shows a quantitative ^{13}C NMR spectrum for a milled wood lignin isolated from a hardwood *Buddleja davidii*. Table 18.2 summarizes signal assignments and chemical shifts of structural features of a spruce milled wood lignin in a ^{13}C NMR measured using deuterated dimethyl sulfoxide (DMSO) as solvent [5,26,27].

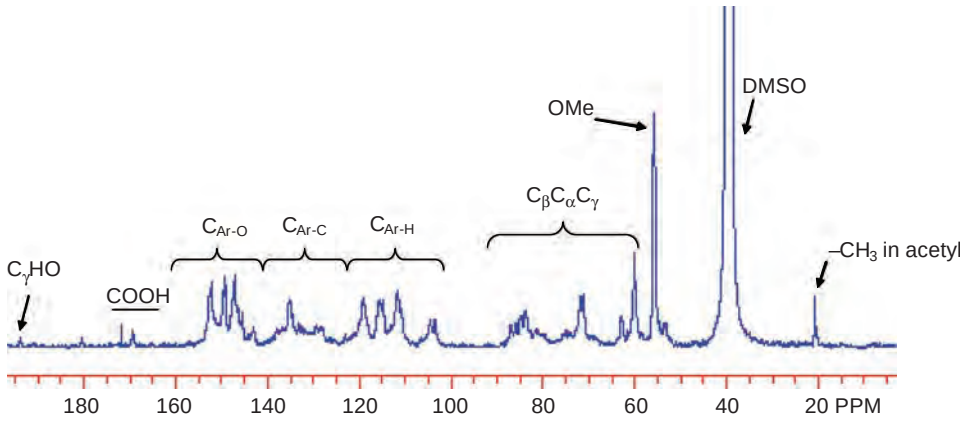

Figure 18.4 *Quantitative ^{13}C NMR spectrum of a milled wood lignin isolated from a hardwood* Buddleja davidii *[28]. Ar: aromatic; OMe: methoxyl; DMSO: dimethyl sulfoxide.*

Hallac *et al.* [28] employed quantitative ^{13}C NMR to characterize structural features of milled wood lignin isolated from a shrub *Buddleja davidii* as a potential feedstock for biofuels production, and reported that the lignin had an approximate guaiacyl/syringyl (G/S) ratio of 81:19 with no H-units observed. They further investigated the chemical transformations of *Buddleja davidii* lignin during ethanol organosolv pretreatment using ^{13}C NMR together with other NMR techniques, and demonstrated quantitative changes of lignin structural features such as substantive decrease of β-O-4 linkages after the pretreatments [29]. Using ^{13}C NMR, Samuel *et al.* [30] observed a 36% decrease in β-O-4 linkages and an S/G ratio decrease from 0.80 to 0.53 for ball-milled lignin isolated from Alamo switchgrass after dilute acid pretreatment. Sannigrahi *et al.* investigated lignin isolated from loblolly pine before and after ethanol organosolv pretreatment and reported a *c.* 50% decrease in β-O-4 linkages utilizing quantitative ^{13}C NMR analysis, suggesting that acid-catalyzed cleavage of β-O-4 linkages was a major mechanism for lignin cleavage [31,32].

18.3.4 HSQC Correlation Spectroscopy

Although 1D ^1H and ^{13}C NMR are very efficient tools for lignin structural analysis, these classical 1D NMR techniques usually suffer from signal overlaps in spectra. With advancements in NMR instrumentation, these issues are now addressed with a host of 2D and 3D NMR techniques, among which HSQC is the most commonly applied. Heteronuclear multidimensional correlation NMR experiments can not only increase the sensitivity of ^{13}C nuclei by polarization transfer but also separate overlapped signals which usually occur in 1D spectra, making ^1H-^{13}C correlation methods very efficient for lignin structural analysis. Indeed, the use of 2D NMR has been instrumental in advancing the analysis of lignin structure, especially in discovering new lignin subunits and the presence of lignin-carbohydrate complexes such as dibenzodioxocin and spirodienone structures [4,17–21]. However, it has limitations in that it is not quantitative and a spectral overlap of lignin functionality still occurs. The application of these techniques to lignin isolated from native as well as genetically altered plants was recently summarized by Ralph *et al.* [33].

HSQC is the most frequently collected 2D NMR spectrum that is used not only for structural identification but also for estimation of the relative abundance of inter-unit linkages as well as S/G ratios in lignin. Table 18.3 summarizes chemical shifts and assignments of cross-peaks of typical inter-unit linkages and/or subunits in HSQC spectra of lignin when using DMSO as solvent. Although this approach

Table 18.3 *Chemical shifts and assignment of ^{13}C-^{1}H correlation signals in HSQC spectra of lignin [34–39].*

δ_C/δ_H (ppm)	Assignment[a]
53.1/3.44	C_β/H_β in phenylcoumaran substructure (B)
53.6/3.03	C_β/H_β in resinol substructure (C)
55.7/3.70	C/H in methoxyl group
59.8/3.62	C_γ/H_γ in β-O-4 ether linkage (A)
61.7/4.09	C_γ/H_γ in cinnamyl alcohol (F)
62.3/4.08,3.95	C_γ/H_γ in dibenzodioxocin
62.8/3.76	C_γ/H_γ in phenylcoumaran substructure (B)
71.1/3.77, 4.13	C_γ/H_γ in resinol substructure (C)
71.4/4.76	C_α/H_α in β-O-4 linked to a G unit (A)
72.1/4.86	C_α/H_α in β-O-4 linked to a S unit (A)
76.0/4.81	C_α/H_α in benzodioxane
78.2/4.00	C_β/H_β in benzodioxane
81.4/5.1	C_β/H_β in spirodienone substructure
83.7/4.31	C_β/H_β in β-O-4 linked to a G unit (A)
84.2/4.69	C_α/H_α in dibenzodioxocin
84.7/4.7	C_α/H_α in spirodienone substructure
85.2/4.63	C_α/H_α in resinol substructure (C)
86.3/4.13	C_β/H_β in β-O-4 linked to a S unit (A)
86.6/4.08	C_β/H_β in dibenzodioxocin
87.0/5.52	C_α/H_α in phenylcoumaran substructure (B)
103.8/6.70	$C_{2,6}/H_{2,6}$ in syringyl units (S)
105.5/7.3	$C_{2,6}/H_{2,6}$ in oxidized syringyl (S′) units with $C_\alpha = O$
111.0/6.98	C_2/H_2 in guaiacyl units (G)
114.8/6.73	$C_{3,5}/H_{3,5}$ in *p*-hydroxyphenyl units (H)
115.1/6.72, 6.98	C_5/H_5 in guaiacyl units
119.1/6.80	C_6/H_6 in guaiacyl units
128.0/7.17	$C_{2,6}/H_{2,6}$ in *p*-hydroxyphenyl units
128.2/6.75	C_β/H_β in cinnamaldehyde unit (E)
128.3/6.45	C_α/H_α in cinnamyl alcohol (F)
128.3/6.25	C_β/H_β in cinnamyl alcohol (F)
130.6/7.65, 7.87	$C_{2,6}/H_{2,6}$ in *p*-hydroxybenzoate units (D)
153.6/7.62	C_α/H_α in cinnamaldehyde unit (E)

[a] G: guaiacyl; S: syringyl; S″ = oxidized syringyl with C_α=O; H: *p*-hydroxyphenyl; A: β-O-4 ether linkage; B: β-5/α-O-4 phenylcoumaran; C: resinol (β-β); D: *p*-hydroxybenzoate; E: cinnamaldehyde; F: cinnamyl alcohol.

is not considered quantitative, it has been widely employed in a semi-quantitative way to offer relative comparisons of inter-unit linkage levels in biomass lignins, such as alfalfa, eucalyptus, and poplar [34–37]. The well-resolved α-carbon contours in various linkages are generally used for volume integration, and the relative abundance of each respective inter-unit linkage is then calculated as the percentage of integrals of total linkages [34,37].

Pu *et al.* [38] recently investigated structural characteristics of lignin isolated from wild-type alfalfa, *p*-coumarate 3-hydroxylase (C3H) down-regulated, and hydroxycinnamoyl CoA:shikimate/quinate hydroxycinnamoyl transferase (HCT) down-regulated alfalfa transgenic lines. The HSQC spectra of lignin in wild-type and transgenic alfalfa shown in Figures 18.5 and 18.6 illustrate ^{1}H-^{13}C correlation signals in aromatic regions and aliphatic side-chain ranges, respectively. The HSQC spectra demonstrated that C3H and HCT down-regulated alfalfa lignins showed significantly more *p*-hydroxyphenyl units along with a substantial

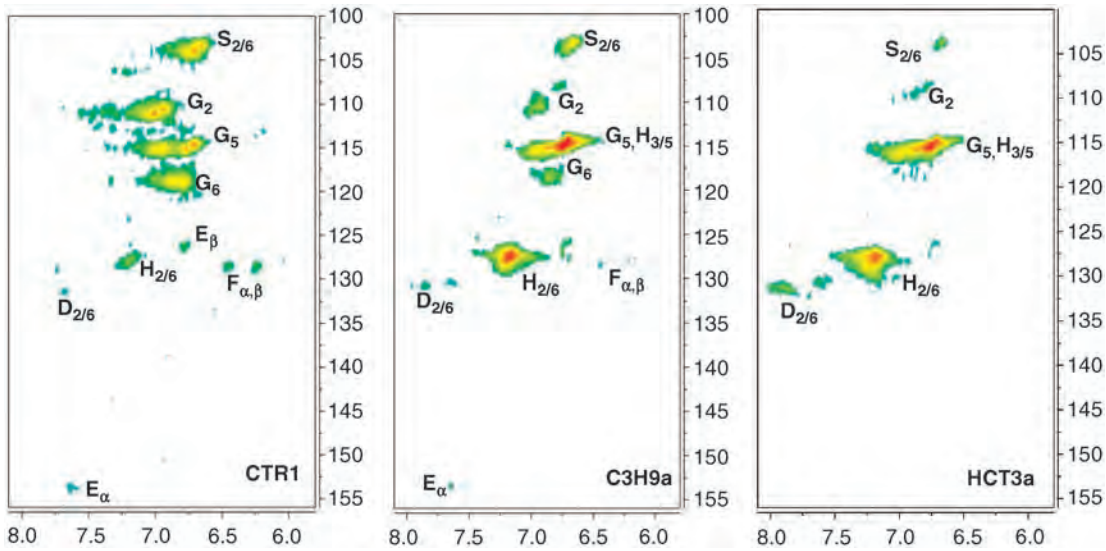

Figure 18.5 *Aromatic regions of $^{13}C/^{1}H$ HSQC NMR spectra of alfalfa ball-milled lignins [38]. G: guaiacyl; S: syringyl; H:* p*-hydroxyphenyl; D:* p*-hydroxybenzoate; E: cinnamaldehyde; F: cinnamyl alcohol. CTR1: wild type; C3H9a:* p*-coumarate 3-hydroxylase (C3H) transgenic line; HCT3a: hydroxycinnamoyl CoA:shikimate/quinate hydroxycinnamoyl transferase (HCT) transgenic line.*

decrease in the intensities of syringyl and guaiacyl correlations. Compared to the wild-type plant, the C3H and HCT transgenic lines had an increased phenylcoumaran and resinol linkages in lignins. Using HSQC NMR, Ralph *et al.* [34] also characterized the structures of acetylated alfalfa lignins isolated from severely down-regulated C3H transgenic lines. They reported structural differences in inter-unit linkage distribution with a decrease in β-aryl ether units, which were accompanied by relatively higher levels of phenylcoumarans and resinols. In addition, Ralph *et al.* [34] provided data for coupling and cross-coupling propensities of *p*-coumaryl alcohol and *p*-hydroxyphenyl units in C3H-deficient alfalfa lignin and revealed that (1) β-ether units were from G, S, and *p*-hydroxyphenyl but with relatively low levels of the G- (especially) and S-units, and (2) the phenylcoumarans were almost entirely from *p*-hydroxyphenyl units. Moinuddin *et al.* [39] investigated lignin structures of *Arabidopsis thaliana* COMT mutant *Atomt1* using HSQC NMR and suggested that β-O-4 linkage frequency in the lignin isolates of both the *Atomt1* mutant and wild-type line was conserved.

18.3.5 ^{31}P NMR Spectroscopy

An approach to deal with the limitations of the general 1D ^{1}H and ^{13}C NMR and 2D correlation NMR techniques is to "selectively tag" specific functional groups in lignin with an NMR active nucleus through derivatization and then analyze the derivatized lignin with NMR. Phosphorous reagents have been employed to tag hydroxyl groups or quinone structures in lignin for determining their concentration by ^{31}P NMR [28–30,40–43]. Hydroxyl groups, especially free phenoxy groups, are among the most important functionalities affecting physical and chemical properties of lignin. These functional groups exhibit a prominent role in defining reactivity of lignin to promote cleavage of inter-unit linkages and/or oxidative degradation during pretreatment processes. The traditional wet chemistry methods employed to determine

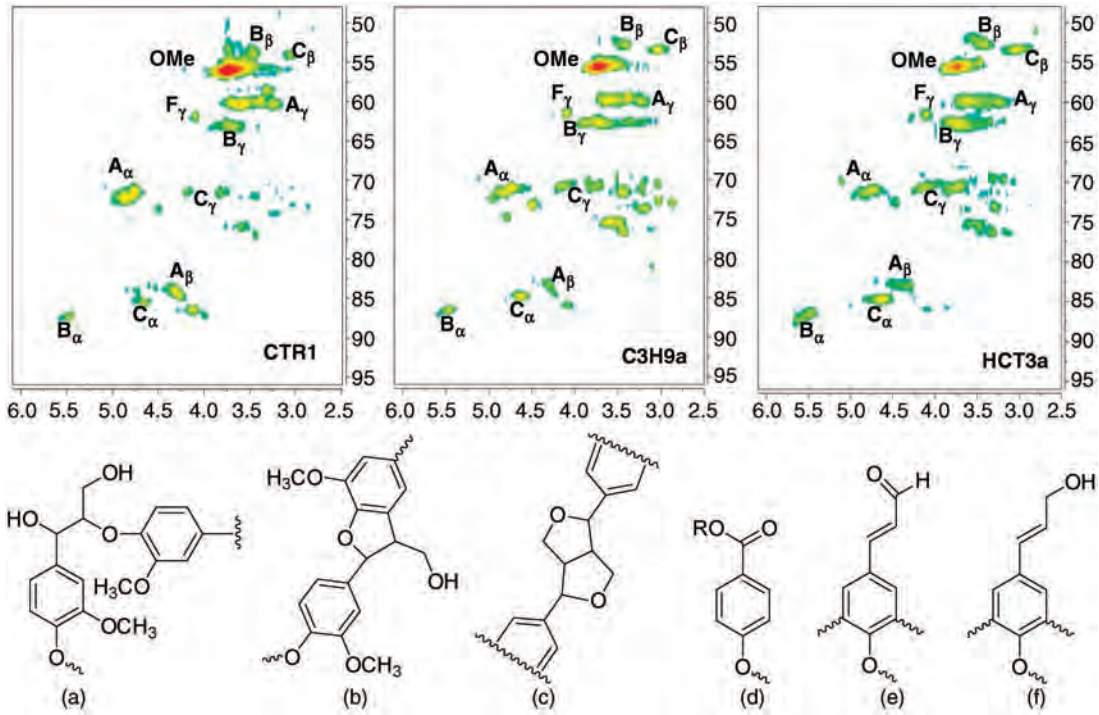

Figure 18.6 *Aliphatic regions of $^{13}C/^{1}H$ HSQC NMR spectra of alfalfa ball-milled lignins and the identified structures [38]. A: β-O-4 ether linkage; B: phenylcoumaran (β-5/α-O-4); C: resinol (β-β); OMe: methoxyl group; D:* p*-hydroxybenzoate; E: cinnamaldehyde; F: cinnamyl alcohol; R = H or C; CTR1: wild type; C3H9a:* p*-coumarate 3-hydroxylase (C3H) transgenic line; HCT3a: hydroxycinnamoyl CoA:shikimate/quinate hydroxycinnamoyl transferase (HCT) transgenic line .*

hydroxyl contents in lignin typically involve time-consuming and/or laborious multistep derivatizations [43]. The ^{31}P NMR method has been shown to be very effective for determining the presence of hydroxyl groups in lignin. It can provide quantitative information in a single spectrum for various types of major hydroxyl groups including aliphatic, carboxylic, guaiacyl, syringyl, C_5-substituted phenolic hydroxyls, and *p*–hydroxyphenyls in a relatively short experimental time and with small sample size requirements. The quantitative information gained from this technique has been verified against other techniques such as GC, ^{1}H NMR, ^{13}C NMR, Fourier transform infrared (FTIR), and wet chemistry methods during an international "round robin" lignin study [44,45]. Compared to ^{1}H NMR, the large range of chemical shifts for ^{31}P nucleus generates a better separation and resolution of signals. In addition, the 100% natural abundance of the ^{31}P and its high sensitivity renders ^{31}P NMR a rapid analytical tool in comparison to ^{13}C NMR.

The ^{31}P NMR technique usually involves treating lignin samples with the phosphorylation reagent 2-chloro-4,4,5,5 tetramethyl-1,3,2-dioxaphospholane (TMDP) to phosphorylate the labile hydroxyl protons in lignin according to the reaction outlined in Figure 18.7. The ^{31}P NMR spectrum of this derivatized sample is then recorded with an internal standard such as cyclohexanol or N-hydroxy-5-norbornene-2,3-dicarboximide. The ^{31}P NMR spectrum contains well-separated peaks corresponding to the various types of hydroxyl groups present in lignin. The fact that these peaks are well separated is very important in making it possible to distinguish between regions containing various types of hydroxyl groups and allow for their

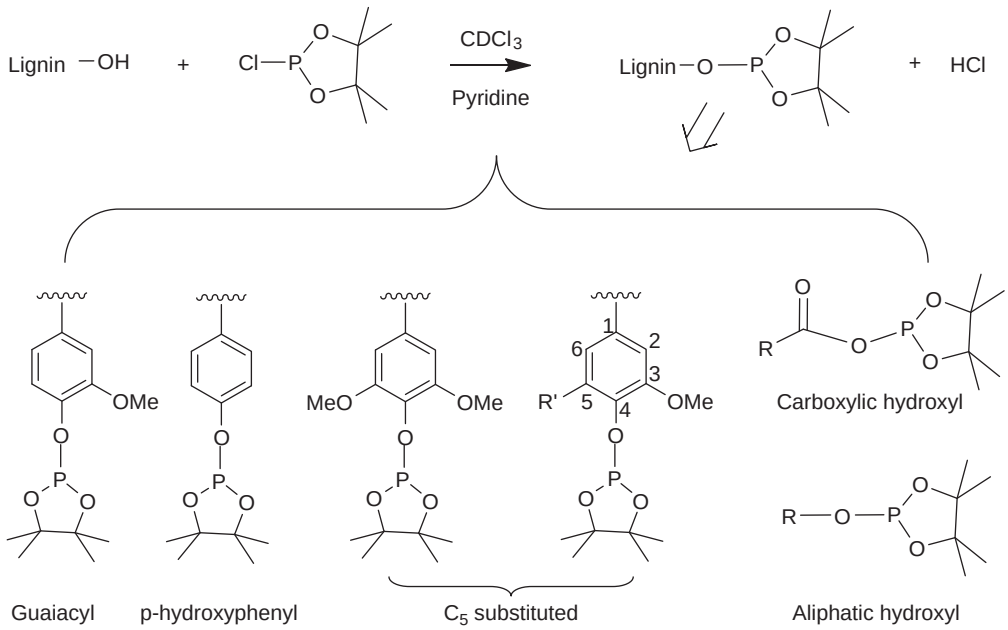

Figure 18.7 *Reaction of labile hydroxyls present in lignins with 2-chloro-4,4,5,5 tetramethyl-1,3,2-dioxaphospholane. R: Lignin side-chain; R′: lignin unit.*

accurate integration. Figure 18.8, which is a ^{31}P NMR spectrum of a hardwood lignin derivatized with 2-chloro-4,4,5,5 tetramethyl-1,3,2-dioxaphospholane, illustrates the well-separated signals arising from the various hydroxyl groups in lignin. A compilation of typical assignments and chemical shifts/integration ranges of hydroxyl groups in lignin using TMDP/^{31}P NMR analysis is shown in Table 18.4 [46].

For ^{31}P NMR analysis of lignin, the solvent employed is usually a mixture of anhydrous pyridine and deuterated chloroform (*c.* 1.6 : 1.0 v/v) containing a relaxation agent (i.e., chromium (III) acetylacetonate) and an internal standard. An accurately weighed dried lignin sample (10–25 mg) is dissolved in a NMR

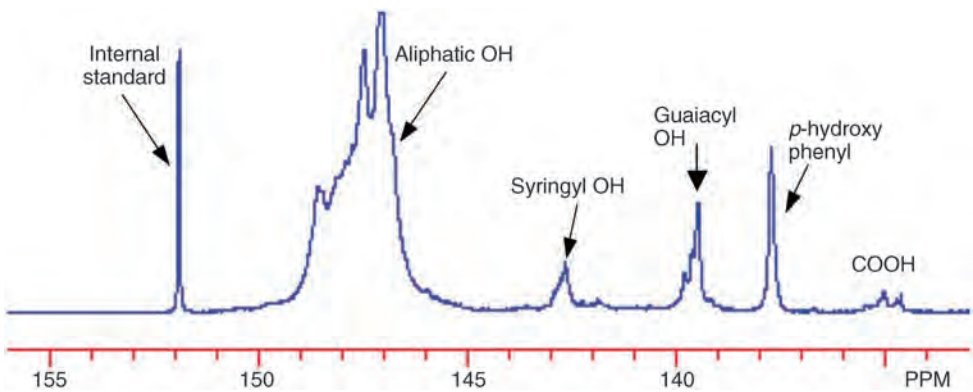

Figure 18.8 *Quantitative ^{31}P NMR spectrum of a hardwood lignin derivatized with TMDP using N-hydroxy-5-norbornene-2,3-dicarboximide as internal standard.*

Table 18.4 *Typical chemical shifts and integration regions for lignins in a ^{31}P NMR spectrum [46].*

δ (ppm)	Assignment
145.4–150.0	Aliphatic OH
137.6–144.0	Phenols
a) 140.2–144.5	C_5 substituted phenols
c. 143.5	β–5
c. 142.7	Syringyl
c. 142.3	4–O–5
c. 141.2	5–5
b) 139.0–140.2	Guaiacyl
c) *c.* 138.9	Catechol
d) *c.* 137.8	*p*–hydroxyphenyl
133.6–136.0	Carboxylic OH

solvent mixture (0.50 mL). TMDP reagent (*c.* 0.05–0.10 mL) is added and stirred for a short period of time at room temperature. Since the derivatization reagent is moisture sensitive, all efforts need to be directed at reducing exposure to water. Quantitative ^{31}P NMR spectra are generally recorded with a long pulse delay which is at least 5 times greater than the longest spin-lattice relaxation time (i.e., T_1) of ^{31}P nucleus to allow phosphorus nuclei to reach thermal equilibrium prior to a subsequent pulse. Chromium (III) acetylacetonate in a solvent system is generally used as a relaxation agent to shorten the spin-lattice relaxation time of phosphorus nuclei. Typically, a 25 s pulse delay is considered appropriate for quantitative ^{31}P NMR analysis of lignin. In addition, an inverse gated decoupling pulse is employed to eliminate nuclear Overhauser effects for quantification. Using a 90° pulse and the conditions above, 128–256 acquisitions (*c.* 1–2 h) at room temperature are sufficient to acquire a spectrum with a satisfactory S/N ratio.

Sannigrahi *et al.* [31,32] employed ^{31}P NMR to characterize ball-milled lignin isolated from loblolly pine and reported that ethanol organosolv pretreatment (EOP) of loblolly pine resulted in an ethanol organosolv lignin (EOL) with a higher content of guaiacyl phenolic, *p*-hydroxyl phenolic, and carboxylic hydroxyl groups. Hallac *et al.* [28,29] applied ^{31}P NMR to determine the hydroxyl content of *Buddleja davidii* lignin during ethanol organosolv pretreatments with various pretreatment severities. Compared to milled wood lignin from native *B. davidii*, the amount of phenolic OH, both condensed and guaiacyl, increased significantly in EOLs. The aliphatic OH groups in *B.* davidii EOLs were observed to decrease in content by 41–59%, and this decrease of aliphatic OH was enhanced as pretreatment severity increased. ^{31}P NMR analysis by El Hage *et al.* [47,48] showed that EOP resulted in a decrease of aliphatic hydroxyl content and an increase in phenolic hydroxyl groups in *Miscanthus* EOLs. Based on the ^{31}P NMR results, together with ^{13}C NMR and FTIR analysis, El Hage *et al.* proposed that EOP resulted in extensive aryl-ether bond hydrolysis of *Miscanthus* lignin and that cleavage of α-aryl ether bonds was the primary reaction responsible for lignin depolymerization [47,48]. Using ^{31}P NMR analysis, Samuel *et al.* [30] documented that dilute-acid pretreatment led to a 27% decrease in aliphatic hydroxyl content and a 25% increase in phenolic hydroxyl content in switchgrass lignin, while the OH content in *p*-hydroxyphenyl and carboxyl remained relatively unchanged. These results provide vivid examples of the use of phosphorus derivatization followed by NMR analysis to characterize the structural nature of lignin in starting and pretreated biomass.

Using ^{31}P NMR methodology, Akim *et al.* [49] investigated structural features of ball-milled lignins isolated from a wild-type control, a cinnamyl alcohol dehydrogenase (CAD) down-regulated line, and a caffeic acid/5-hydroxyferulic acid O-methyl transferase (COMT) down-regulated transgenic poplar. According to the ^{31}P NMR results, Akim *et al.* [49] documented that moderate CAD down-regulation (70%

deficient) resulted in no drastic changes in structures of poplar lignin. More severe CAD depletion for 6-month old poplar led to a slight increase in the amount of condensed phenolic hydroxyls, which the authors suggested was indicative of a higher degree of cross-linked lignin. Compared to the wild-type control, COMT down-regulation (90% deficient) yielded a poplar lignin with a lower content of syringyl and aliphatic OH group as well as an increased guaiacyl phenolic OH amount, while *p*-hydroxyphenyl and carboxylic OH content was observed to remain unchanged after COMT down-regulation [49].

18.4 Solid-state NMR Characterization of Plant Cellulose

18.4.1 CP/MAS ^{13}C NMR Analysis of Cellulose

Since the early 1980s, the solid-state CP/MAS ^{13}C NMR technique has been widely applied for investigation of structural features of cellulose, providing not only information of crystallinity index but also enabling a thorough investigation of the ultrastructure of cellulose [50,51]. Cellulose is a linear polymer made up of β-D glucopyranose units covalently linked by $1 \rightarrow 4$ glycosidic bonds, with the degree of polymerization varying with the biomass source [10,52]. Figure 18.9 illustrates the molecular structure of cellulose [52].

The large number of hydroxyl groups on cellulose chains form intra- and inter-molecular hydrogen bonds, resulting in the crystalline structure of cellulose. Cellulose also has a less-ordered structure called amorphous cellulose. Native crystalline cellulose (cellulose I) has been shown to co-exist in the form of two allomorphs (i.e., I_α and I_β) [50]. The degree of cellulose crystallinity has been studied over the years for many species, and a term called crystallinity index (CrI) is widely used to represent the relative proportion of crystalline cellulose to the total cellulose present in a material. The two most common techniques used to measure this value are X-ray diffraction (XRD) and solid-state CP/MAS ^{13}C NMR. XRD is based on the concept that the X-ray scattering can be divided into two components due to crystalline and amorphous structures [53]. Table 18.5 presents the degree of crystallinity of several cellulose samples measured by XRD [10,11,53].

The cellulose sample for solid-state CP/MAS ^{13}C NMR is usually ground and packed into a MAS rotor which is then inserted into a MAS probe and spun at a frequency of 5–10 kHz. CP/MAS ^{13}C NMR measurements are generally carried out with a 90° proton pulse, 0.8–2.0 ms contact pulse, 4 s recycle delay, and 2024–8192 scans for a good S/N ratio. The spectra are usually recorded on moist samples (*c.* 30–60% water content) to increase signal resolution. The solid-state CP/MAS ^{13}C NMR technique to measure the crystallinity of cellulose is based on the intensity of the two peaks in the C-4 region (δ *c.* 80–92 ppm): the first peak corresponds to the crystalline structure (δ = 86–92 ppm), whereas the amorphous region is located in the range of δ = 80–86 ppm. This method is referred to as the C-4 peak separation NMR technique. In order for this technique to be accurate, hemicelluloses and lignin must be removed from the cellulose samples because they interfere with the area of the amorphous region [54]. Figure 18.10 shows a typical CP/MAS ^{13}C NMR spectrum of a cellulose sample isolated from switchgrass. Cellulose crystallinity values for various lignocellulosic materials measured by this method are summarized in Table 18.6 [7,28,31,55,56].

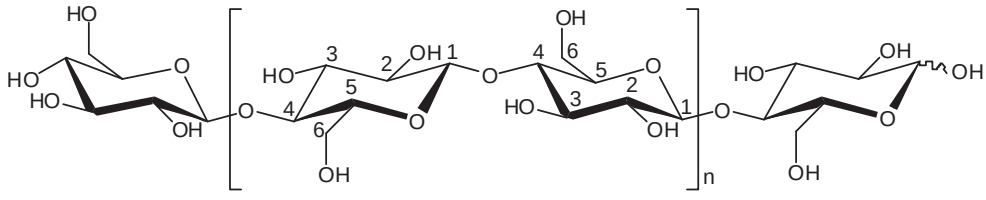

Figure 18.9 *Molecular structure of cellulose [52].*

Table 18.5 *Crystallinity index of some cellulosic materials determined by XRD [10,11,53].*

Sample	Crystallinity index (%)
Cotton linters	50–63
Wood pulp	50–70
Viscose rayon	27–40
Regenerated cellulose film	40–45
Avicel	50–60
Cotton	81–95
Algal cellulose	>80
Bacterial cellulose	65–79
Ramie	44–47

Table 18.6 *Crystallinity index of some cellulosic materials measured by C-4 peak separation NMR technique [7,28,31,55,56].*

Sample	Crystallinity index (%)
Hybrid poplar	63
Loblolly pine	63
Switchgrass alamo	44
Buddleja davidii	55
Spruce	48
Birch	36

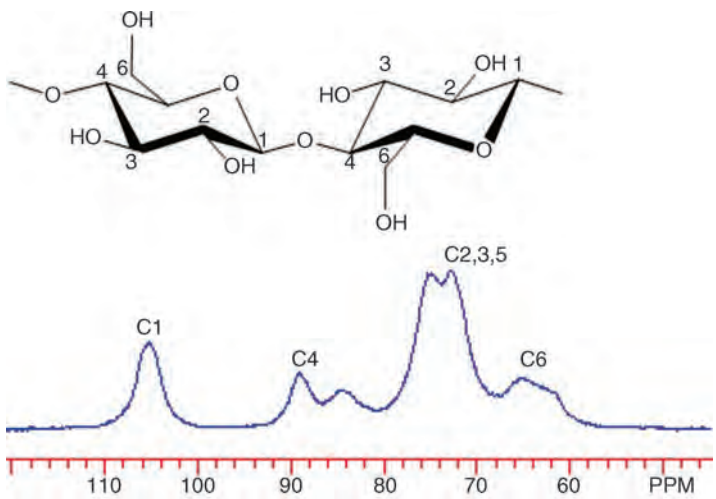

Figure 18.10 *CP/MAS ^{13}C-NMR spectra of cellulose isolated from switchgrass.*

In a recent study by Park *et al.*, a new NMR technique to measure cellulose crystallinity was introduced [57]. This novel method is based on digitally subtracting the spectrum of standard amorphous cellulose from the original spectrum. The authors believe that this method is straightforward, easier than XRD and C-4 peak separation methods, and could be applied to cellulose with any level of crystallinity [57].

The current interest in determining the degree of crystallinity of cellulose is to correlate the relationship between changes in CrI during pretreatment to the efficiency of enzymatic hydrolysis in the biological process of converting cellulosic biomass to biofuels. It is believed that cellulose crystallinity is a key property contributing to biomass recalcitrance [58]. Lowering cellulose crystallinity should therefore make it more readily digestible by cellulase. However, it has been suggested in various studies that changes in crystallinity after pretreatment and its effect on the enzymatic hydrolysis are related to the nature of the original material as well as the pretreatment technologies employed. Therefore, crystallinity index itself may not provide enough information to explain enzymatic hydrolysis behavior. Greater importance needs to be assigned to the ultrastructure of cellulose and not just to crystallinity in general.

18.4.2 Cellulose Crystallinity

In the realm of the utilization of cellulose as a material and as a feedstock for biofuels production, many studies have examined the effect of pretreatment on the crystallinity of cellulose. Table 18.7 [56–63] summarizes the CrI of cellulose of various untreated and pretreated biomass after some pretreatment processes such as ammonia fiber expansion (AFEX), ammonia recycled percolation (ARP), controlled pH, dilute sulfuric acid, lime, SO_2, ozone (O_3), carbon dioxide explosion (CE), alkaline explosion (AE), and organosolv.

As to be expected, each pretreatment had a different effect on cellulose crystallinity. Some pretreatment technologies caused a reduction in cellulose crystallinity, some showed no effect on crystallinity, and others exhibited an increase in crystallinity. Low-pH pretreatments generally enriched biomass crystallinity, while all high-pH pretreatments had less effect and even reduced biomass crystallinity in some instances. It also appears that the effect of the same pretreatment is biomass-dependent. For instance, controlled-pH pretreatment (i.e., controlling the pH at near neutral conditions) reduced the crystallinity index of corn stover, while it caused an increase in crystallinity of poplar. In general, dilute acid, lime, CO_2 explosion, alkaline explosion, and SO_2 pretreatments increased cellulose crystallinity due to the fact that amorphous cellulose degrades more easily than the more stable crystalline cellulose during pretreatment. Pretreatments such as AFEX, ARP, and ethanol organosolv are capable of reducing the crystallinity of cellulose, suggesting possible decrystallization of cellulose. Furthermore, the resulting crystallinity of pretreated biomass depends on the pretreatment conditions employed. Table 18.8 shows that lodgepole pine cellulose crystallinity increased when the pretreatment severity increased from condition set 1 to 3, causing an enrichment in the crystalline form of cellulose due to selective hydrolysis of amorphous cellulose during pretreatment [64].

Since cellulose crystallinity is thought to be a key property contributing to plant recalcitrance, many studies have focused on establishing a correlation between crystallinity and enzymatic hydrolysis of cellulose. A study by Jeoh *et al.* demonstrated the effect of cellulose crystallinity on cellulase accessibility [58]. Amorphous cellulose samples were prepared from Avicel and filter paper as follows. Cellulose was dissolved in a dimethylsulfoxide-paraformaldehyde solution, and then regenerated by slow addition of the cellulose solution to a solution of 0.2 M sodium alkoxide in methanol/i-propanol (1 : 1). This procedure has been demonstrated to produce amorphous cellulose without altering the degree of polymerization (DP) and reducing end-group concentration of the starting cellulose [58,65]. The resulting amorphous forms of cellulose were found to be significantly more digestible by cellulase than the original crystalline forms. For both Avicel and filter paper, the extent of cellulose hydrolysis increased from 10% to 80% for crystalline and amorphous forms, respectively [58]. Specifically, the bound cellulase concentrations on the amorphous

Table 18.7 *Crystallinity index of several untreated and pretreated biomass cellulose using various pretreatment technologies.*

Biomass	Pretreatment	Crystallinity index (%)
Corn stover[a,] [59]	—	50.3
	Ammonia fiber expansion	36.3
	Ammonia recycled percolation	25.9
	Controlled pH	44.5
	Dilute Acid	52.5
	Lime	56.2
Poplar[a,] [59]	—	49.9
	Ammonia fiber expansion	47.9
	Ammonia recycled percolation	49.5
	Controlled pH	54.0
	Dilute acid	50.6
	Lime	54.5
	SO_2	56.5
Bagasse[a,] [60]	—	37
	O_3	38
	CO_2 explosion	57
	Alkaline explosion	62
Wheat straw[a,] [60]	—	35
	O_3	34
	CO_2 explosion	56
	Alkaline explosion	53
Eucalyptus regnans [a,] [60]	—	37
	O_3	40
	CO_2 explosion	53
Pinus radiata [a,] [60]	—	34
	O_3	36
Switchgrass[a,] [61]	—	46.1
	Lime	51.9
Loblolly pine[b,] [31,62]	—	62.5
	Dilute acid	69.9
	Ethanol organosolv	53
Buddleja davidii [b,] [63]	—	55
	Ethanol organosolv	49

[a] CrI measured by X-ray diffraction.
[b] CrI measured by CP/MAS ^{13}C NMR.

Table 18.8 *Crystallinity index of ethanol-organosolv-pretreated substrates prepared from lodgepole pine under various conditions.*

Condition	Temperature (°C)	Time (min)	Sulfuric acid dosage (%)	Concentration of ethanol (%)	Crystallinity index (%)
1	170	60	0.76	65	75
2	170	60	1.10	65	78
3	180	60	1.10	65	85

forms of both filter paper and Avicel were significantly higher than on the crystalline forms (i.e., 0.1 μmoles/g of remaining cellulose for the crystalline form and 1.5 μmoles/g of remaining cellulose for the amorphous form) [58]. The maximum extents of binding on the amorphous forms increased by a factor of 15 over that of the original forms. The change in crystallinity of the cellulose samples may therefore have allowed increased access to cellulase [58]. It could therefore be inferred that the increased access may have contributed to the increased cellulose hydrolysis rates observed. Another study by Zhu *et al.* illustrated the relationship between biomass digestibility and crystallinity. Hybrid poplar was treated with varying amounts of peracetic acid and KOH to generate samples with different crystallinity [66]. The results clearly indicated that the enzymatic digestibility of the biomass increased with decreasing biomass crystallinity, suggesting that amorphous cellulose is more accessible to enzymatic digestibility.

18.4.3 Cellulose Ultrastructure

To further understand the effects of pretreatments on biomass enzymatic digestibility, the changes in the ultrastructure of cellulose and how it is affected by pretreatment need to be investigated. The ultrastructure of cellulose has long been studied by CP/MAS ^{13}C NMR. Atalla and VanderHart were among the first to apply this NMR technique and concluded that native cellulose in plants has two crystalline allomorphs: cellulose I_α and cellulose I_β [50]. Cellulose I_α, a one-chain triclinic unit cell, is the dominant form in bacterial and algal cellulose; cellulose I_β, a monoclinic two-chain unit cell, is dominant in higher plants such as cotton, ramie, and wood [67]. By annealing, the meta-stable cellulose I_α can be converted to the thermodynamically more stable cellulose I_β [68]. Nishiyama *et al.* proposed that slippage of the glucan chains is the most likely mechanism for conversion of cellulose I_α to cellulose I_β [69]. Solid-state CP/MAS ^{13}C NMR of cellulose has been shown to be a convenient analytical technique to characterize several other forms of cellulose such as *para*-crystalline cellulose, and two non-crystalline forms: amorphous cellulose at accessible and inaccessible fibril surfaces [54,67,70,71]. *para*-Crystalline cellulose is the form that is less ordered than cellulose I_α and cellulose I_β, but more ordered than amorphous cellulose [67]. Accessible fibril surfaces are those in contact with water/solvent, while the inaccessible fibril surfaces are fibril-fibril contact surfaces and surfaces resulting from distortions in the fibril interior [31]. In order to analyze and quantify these various crystalline allomorphs and amorphous domains, Larsson *et al.* developed a model and methodology based on non-linear spectral fitting with a combination of Lorentzian and Gaussian functions [70,72]. Figure 18.11 shows the spectral fitting of C-4 region of the solid-state CP/MAS ^{13}C NMR spectrum of cellulose isolated from *Buddleja davidii*, and the assignments of signals and fitting parameters are presented in Table 18.9 [28].

Table 18.9 *Assignments of signals in the C-4 region of CP/MAS ^{13}C NMR spectrum obtained from Buddleja davidii cellulose.*

Assignments	Chemical shift (ppm)	FWHH[a] (Hz)	Intensity (%)	Line type
Cellulose I_α	89.6	96	4.2	Lorentz
Cellulose $I_{\alpha+\beta}$	88.9	85	8.7	Lorentz
Para-crystalline cellulose	88.7	258	32.9	Gauss
Cellulose I_β	88.2	142	6.5	Lorentz
Accessible fibril surface	84.6	116	3.9	Gauss
Inaccessible fibril surface	84.1	482	41.1	Gauss
Accessible fibril surface	83.6	101	2.7	Gauss

[a] FWHH: Full width at half-height.

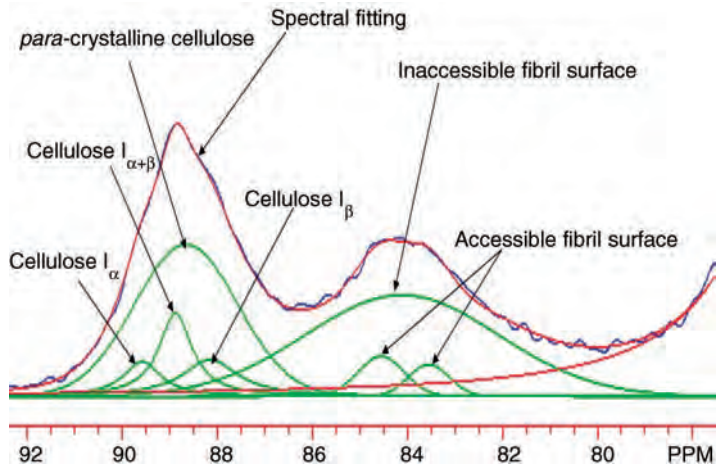

Figure 18.11 *Spectral fitting for the C-4 region of CP/MAS ^{13}C-NMR spectrum of native Buddleja davidii cellulose [28]. $I_{\alpha+\beta}$: $I(\alpha+\beta)$*

A study by Pu *et al.* [67] showed that cellulose I_α, *para*-crystalline, and amorphous celluloses of fully bleached softwood (pine) kraft pulp are more susceptible to enzymatic hydrolysis than cellulose I_β, which is the more ordered and stable crystal structure. Since cellulose I_β is the predominant form in wood, it is of great importance for pretreatment technologies to convert the I_β allomorph to the more easily digestible *para*-crystalline and amorphous celluloses. In another study, Sannigrahi *et al.* [62] showed that the CrI of ethanol-organosolv-pretreated loblolly pine cellulose increased by 53% after treatment with cellulase and that the relative intensities of amorphous and *para*-crystalline cellulose decreased, suggesting that enzymes selectively degrade these forms of cellulose. In contrast, Cateto *et al.* [73] reported recently that the crystallinity of ethanol-organosolv-pretreated Kanlow switchgrass remained approximately constant upon enzymatic hydrolysis by cellulase. The explanation for such results was hypothesized to be by the effect of the synergistic action of endo- and exoglucanases on the removal of the outer layers of the cellulose crystallite in order to gain access to the inner layers, characteristic of a "peeling-off" type mechanism [73]. It therefore appears that the impact of enzymatic hydrolysis on the crystallinity of cellulose is dependent, to some extent, on the nature/structure of the cellulosic substrate.

The effects of dilute acid and organosolv pretreatment on the ultrastructure of various cellulosic materials are summarized in Table 18.10 [7,31,62,63]. The data indicate that the main difference between

Table 18.10 *Variations in the ultrastructure of cellulose after pretreatment [7,31,62,63].*

Species	Pretreatment	Changes in ultrastructure of cellulose[a]		
		I_β	*Para*-crystalline	Amorphous
Loblolly pine	Dilute acid	+	−	−
Loblolly pine	Ethanol organosolv	+	−	+
Switchgrass	Dilute acid	+	+	−
Buddleja davidii	Ethanol organosolv	−	+	+

[a] + indicates increase and − indicates decrease in the specific cellulosic structure.

pretreatments is the ability of ethanol organosolv pretreatment to increase the amorphous regions of pine and *Buddleja davidii* cellulose, which could possibly improve enzymatic hydrolysis. Dilute-acid pretreatment increased cellulose I_β, an observation that can be explained by the thermal conversion of cellulose I_α to the more stable cellulose I_β, or simply an enrichment in the crystalline structure after hydrolysis of the amorphous structures. The results clearly show that the variations in cellulose ultrastructure are pretreatment dependent and related to the nature of the origin of the cellulosic material.

18.5 Future Perspectives

The solution- and solid-state NMR techniques presented in this chapter offer powerful and effective tools for analysis of lignin and cellulose for biomass characterization. Given the importance and need for thorough analysis of the fundamental structures of plant biomass as well as its conversion chemistry in aqueous pretreatments for biological and chemical conversion to fuels and chemicals, these methods can and will continue to have broad applicability for researchers involved in biomass conversion to second- and third-generation biofuels in the future.

Acknowledgements

This work was supported and performed as part of the BioEnergy Science Center (BESC). The BioEnergy Science Center is a US Department of Energy Bioenergy Research Center supported by the Office of Biological and Environmental Research in the DOE Office of Science.

References

1. Yang, B. and Wyman, C.E. (2008) Pretreatment: the key to unlocking low-cost cellulosic ethanol. *Biofuels, Bioproducts, and Biorefining*, **2**, 26–40.
2. Ralph, J. and Landucci, L.L. (2010) NMR of lignins, in *Lignin and Lignans* (eds C. Heitner, D.R. Dimmel, and J.A. Schmidt), CRC Press, Boca Raton, Fla, pp. 137–244.
3. Anterola, A.M. and Lewis, N.G. (2002) Trends in lignin modification: a comprehensive analysis of the effects of genetic manipulations/mutations on lignification and vascular integrity. *Phytochemistry*, **61** (3), 221–294.
4. Balakshin, M.Y., Capanema, E.A., and Chang, H.M. (2007) MWL fraction with a high concentration of lignin-carbohydrate linkages: isolation and 2D NMR spectroscopic analysis. *Holzforschung*, **61**, 1–7.
5. Robert, D. (1992) Carbon-13 nuclear magnetic resonance spectroscopy, in *Methods in Lignin Chemistry* (eds S.Y. Lin and C.W. Dence), Springer-Verlag, New York, NY, pp. 250–273.
6. Ludwig, C., Nist, B., and McCarthy, J.L. (1964) The high resolution nuclear magnetic resonance spectroscopy of protons in acetylated lignins. *Journal of the American Chemical Society*, **86**, 1196–1202.
7. Samuel, R., Pu, Y., Foston, M., and Ragauskas, A.J. (2010) Solid-state NMR characterization of switchgrass cellulose after dilute acid pretreatment. *Biofuels*, **1**, 85–90.
8. Lundquist, K. (1992) Proton (^{1}H) NMR spectroscopy, in *Methods in Lignin Chemistry* (eds S.Y. Lin and C.W. Dence) Springer-Verlag, New York, NY, pp. 242–249.
9. Ragauskas, A.J., Williams, C.K., Davison, B.H. *et al.* (2006) The path forward for biofuels and biomaterials. *Science*, **311**, 484–489.
10. Klemm, D., Heublein, B., Fink, H.-B., and Bohn, A. (2005) Cellulose: Fascinating biopolymer and sustainable raw material. *Angewandte Chemie-International Edition*, **44**, 3358–3393.
11. Pu, Y., Zhang, D., Singh, P.M., and Ragauskas, A.J. (2007) The new forestry biofuels sector. *Biofuels, Bioproducts, and Biorefining*, **2**, 58–73.
12. Harris, P.J. and Stone, B.A. (2008) Chemistry and molecular organization of plant cell walls, in *Biomass Recalcitrance: Deconstructing the Plant Cell Wall for Bioenergy* (ed. M.E. Himmel), Blackwell, pp. 61–93.

13. Sjöström, E. (1993) *Wood Chemistry: Fundamentals and Applications*, 2nd edn, Academic Press, New York, NY.
14. Boerjan, W., Ralph, J., and Baucher, M. (2003) Lignin biosynthesis. *Annual Review of Plant Biology*, **54**, 519–546.
15. Davin, L.B. and Lewis, N.G. (2005) Lignin primary structures and dirigent sites. *Current Opinion in Biotechnology*, **16**, 407–415.
16. Chakar, F.S. and Ragauskas, A.J. (2004) Review of current and future softwood kraft lignin process chemistry. *Industrial Crops and Products*, **20**, 131–141.
17. Brunow, G., Kilpelainen, I., Sipila, J. *et al.* (1998) Oxidative coupling of phenols and the biosynthesis of lignin, in *ACS Symposium Series, 697 (Lignin and Lignan Biosynthesis)*, American Chemical Society.
18. Karhunen, P., Rummakko, P., Sipila, J., and Brunow, G. (1995) Dibenzodioxocins: a novel type of linkage in softwood lignins. *Tetrahedron Letters*, **36**, 169–170.
19. Kukkola, E.M., Koutaniemi, S., Pollanen, E. *et al.* (2004) The dibenzodioxocin lignin substructure is abundant in the inner part of the secondary wall in Norway spruce and silver birch xylem. *Planta*, **218**, 497–500.
20. Zhang, L. and Gellerstedt, G. (2001) NMR observation of a new lignin structure, a spiro-dienone. *Chemical Communications*, **24**, 2744–2745.
21. Zhang, L., Gellerstedt, G., Ralph, J., and Lu, F. (2006) NMR studies on the occurrence of spirodienone structures in lignins. *Journal of Wood Chemistry and Technology*, **26**, 65–79.
22. Bjorkman, A. (1954) Isolation of lignin from finely divided wood with neutral solvents. *Nature*, **174**, 1057–1058.
23. Chang, H.M., Cowling, E.B., Brown, W. *et al.* (1975) Comparative studies on cellulolytic enzyme lignin and milled wood lignin of sweetgum and spruce. *Holzforschung*, **29**, 153–159.
24. Wu, S. and Argyropoulos, D.S. (2003) An improved method for isolating lignin in high yield and purity. *Journal of Pulp and Paper Science*, **29**, 235–240.
25. Li, S. and Lundquist, K. (1994) A new method for the analysis of phenolic groups in lignins by ^{1}H-NMR spectrometry. *Nordic Pulp and Paper Research Journal*, **3**, 191–195.
26. Drumond, M., Aoyama, M., Chen, C.-L., and Robert, D. (1989) Substituent effects on C-13 chemical shifts of aromatic carbons in biphenyl type lignin model compounds. *Journal of Wood Chemistry and Technology*, **9**, 421–411.
27. Pan, X., Lachenal, D., Neirinck, V., and Robert, D. (1994) Structure and reactivity of spruce mechanical pulp lignins IV: ^{13}C-NMR spectral studies of isolated lignins. *Journal of Wood Chemistry and Technology*, **14**, 483–506.
28. Hallac, B.B., Sannigrahi, P., Pu, Y. *et al.* (2009) Biomass characterization of Buddleja davidii: A potential feedstock for biofuel production. *Journal of Agricultural and Food Chemistry*, **57**, 1275–1281.
29. Hallac, B.B., Pu, Y., and Ragauskas, A.J. (2010) Chemical transformations of Buddleja davidii lignin during ethanol organosolv pretreatment. *Energy & Fuels*, **24**, 2723–2732.
30. Samuel, R., Pu, Y., Raman, B., and Ragauskas, A.J. (2010) Structural characterization and comparison of switchgrass lignin before and after dilute acid pretreatment. *Applied Biochemistry and Biotechnology*, **162**, 62–74.
31. Sannigrahi, P., Ragauskas, A.J., and Miller, S.J. (2008) Effects of two-stage dilute acid pretreatment on the structure and composition of lignin and cellulose in loblolly pine. *Bioenergy Research*, **1**, 205–214.
32. Sannigrahi, P., Ragauskas, A.J., and Miller, S.J. (2010) Lignin structural modifications resulting from ethanol organosolv treatment of loblolly pine. *Energy & Fuels*, **24**, 683–689.
33. Ralph, J., Marita, J.M., Ralph, S.A. *et al.* (1999) Solution state NMR of lignins, in *Advances in Lignocellulosics Characterization*, Tappi Press, Atlanta, GA.
34. Ralph, J., Akiyama, T., Kim, H. *et al.* (2006) Effects of coumarate 3-hydroxylase down-regulation on lignin structure. *The Journal of Biological Chemistry*, **281**, 8843–8853.
35. Rencoret, J., Marques, G., Gutierrez, A. *et al.* (2008) Structural characterization of milled wood lignins from different eucalypt species. *Holzforschung*, **62**, 514–526.
36. del Río, J.C., Rencoret, J., Marques, G. *et al.* (2008) Highly acylated (acetylated and/or p-coumaroylated) native lignins from diverse herbaceous plants. *Journal of Agricultural and Food Chemistry*, **56**, 9525–9534.
37. Stewart, J.J., Akiyama, T., Chapple, C. *et al.* (2009) The effects on lignin structure of overexpression of ferulate 5-hydroxylase in hybrid poplar. *Plant Physiology*, **150**, 621–635.
38. Pu, Y., Chen, F., Ziebell, A. *et al.* (2009) NMR characterization of C3H and HCT down-regulated alfalfa lignin. *Bioenergy Research*, **2**, 198–208.

39. Moinuddin, S.G.A., Jourdes, M., Laskar, D.D. *et al.* (2010) Insights into lignin primary structure and deconstruction from Arabidopsis thaliana COMT (caffeic acid O-methyl transferase) mutant Atomt1. *Organic and Biomolecular Chemistry*, **8**, 3928–3946.
40. Zawadzki, M., Runge, T.M., and Ragauskas, A.J. (2000) Facile detection of ortho- and para-quinone structures in residual kraft lignin by phosphorus-31 NMR spectroscopy. *Journal of Pulp and Paper Science*, **26**, 102–106.
41. Granata, A. and Argyropoulos, D.S. (1995) 2-Chloro-4,4,5,5-tetramethyl-1,3,2-dioxaphospholane, a reagent for the accurate determination of the uncondensed and condensed phenolic moieties in lignins. *Journal of Agricultural and Food Chemistry*, **43**, 1538–1544.
42. Argyropoulos, D.S. (2010) Heteronuclear NMR Spectroscopy of Lignins, in *Lignin & Lignans; Advances in Chemistry* (eds C. Heitner, D. Dimmel, and J. Schmidt), CRC Press, pp. 245–265.
43. Lai, Y.-Z. (1992) Determination of phenolic hydroxyl groups, in *Methods in Lignin Chemistry* (eds S.Y. Lin and C. W. Dence), Springer-Verlag, New York, NY, pp. 423–434.
44. Faix, O., Andersons, B., Argyropoulos, D.S., and Robert, D. (1995) Quantitative determination of hydroxyl and carbonyl groups of lignins – an overview. Proceedings of 8th International Symposium on Wood and Pulping Chemistry, Gummerus Kirjapaino Oy, Jyvaskyla, Finland, Vol. 1, pp. 559–566.
45. Faix, O., Argyropoulos, D.S., Robert, D., and Neirinck, V. (1994) Determination of hydroxyl groups in lignins evaluation of ^{1}H-, ^{13}C-, ^{31}P-NMR, FTIR and wet chemical methods. *Holzforschung*, **48**, 387–394.
46. Zawadzki, M. (1999) Quantitative determination of quinone chromophore changes during ECF bleaching of kraft pulp. Ph.D. thesis, Institute of Paper Science and Technology, Atlanta.
47. El Hage, R., Brosse, N., sannigrahi, P., and Ragauskas, A. (2010) Effects of process severity on the chemical structure of Miscanthus ethanol organosolv lignin. *Polymer Degradation and Stability*, **95**, 997–1003.
48. El Hage, R., Brosse, N., Chrusciel, L. *et al.* (2009) Characterization of milled wood lignin and ethanol organosolv lignin from miscanthus. *Polymer Degradation and Stability*, **94**, 1632–1638.
49. Akim, L.G., Argyropoulos, D.S., Jouanin, L. *et al.* (2001) Quantitative phosphorus-31 NMR spectroscopy of lignins from transgenic poplars. *Holzforschung*, **55**, 386–390.
50. Atalla, R.H. and VanderHart, D.L. (1984) Native cellulose: A composite of two distinct crystalline forms. *Science*, **223**, 283–285.
51. Atalla, R.H. (1999) Celluloses, in *Comprehensive Natural Products Chemistry: Carbohydrates and their Derivatives Including Tannins, Cellulose, and Related Lignins*, vol **3** (ed. B.M. Pinto), Elsevier, Amsterdam, pp. 529–598.
52. Hallac, B.B. and Ragauskas, A.J. (2011) Analyzing cellulose degree of polymerization and its relevancy to cellulosic ethanol. *Biofuels, Bioproducts, and Biorefining*, **5**, 215–225.
53. Zhang, Y.P. and Lynd, L.R. (2004) Toward an aggregated understanding of enzymatic hydrolysis of cellulose: Noncomplexed cellulase systems. *Biotechnology and Bioengineering*, **88**, 797–824.
54. Wickholm, K., Larsson, P.T., and Iversen, T. (1998) Assignment of non-crystalline forms in cellulose I by CP/MAS carbon-13 NMR spectroscopy. *Carbohydrate Research*, **312**, 123–129.
55. Sannigrahi, P., Ragauskas, A.J., and Tuskan, G.A. (2010) Poplar as a feedstock for biofuels: A review of compositional characteristics. *Biofuels, Bioproducts, and Biorefining*, **4**, 209–226.
56. Foston, M., Hubbell, C.A., Davis, M., and Ragauskas, A.J. (2009) Variations in cellulosic ultrastructure of poplar. *Bioenergy Research*, **2**, 193–197.
57. Park, S., Johnson, D.K., Ishizawa, C.I. *et al.* (2009) Measuring the crystallinity index of cellulose by solid state ^{13}C nuclear magnetic resonance. *Cellulose*, **16**, 641–647.
58. Jeoh, T., Ishizawa, C.I., Davis, M.F., Himmel, M.E., Adney, W.S. and Johnson, D.K. (2007) Cellulase digestibility of pretreated biomass is limited by cellulose accessibility. *Biotechnology and Bioengineering*, **98**, 112–122.
59. Kumar, R., Mago, G., Balan, V., and Wymand, C.E. (2009) Physical and chemical characterizations of corn stover and poplar solids resulting from leading pretreatment technologies. *Bioresource Technology*, **100**, 3948–3962.
60. Puri, V.P. (1984) Effect of crystallinity and degree of polymerization of cellulose on enzymatic saccharification. *Biotechnology and Bioengineering*, **26**, 1219–1222.
61. Chang, V.S. and Holtzapple, M.T. (2000) Fundamental factors affecting biomass enzymatic reactivity. *Applied Biochemistry and Biotechnology*, **84–86**, 5–37.
62. Sannigrahi, P., Miller, S.J., and Ragauskas, A.J. (2010) Effects of organosolv pretreatment and enzymatic hydrolysis on cellulose structure and crystallinity in Loblolly pine. *Carbohydrate Research*, **345**, 965–970.

63. Hallac, B.B., Sannigrahi, P., Pu, Y. *et al.* (2010) Effect of ethanol organosolv pretreatment on enzymatic hydrolysis of Buddleja davidii stem biomass. *Industrial & Engineering Chemistry Research*, **49**, 1467–1472.
64. Pan, X., Xie, D., Yu, R.W., and Saddler, J.N. (2008) The bioconversion of mountain pine beetle-killed lodgepole pine to fuel ethanol using the organosolv process. *Biotechnology and Bioengineering*, **101**, 39–48.
65. Schroeder, L.R., Gentile, V.M., and Atalla, R.H. (1986) Nondegradative preparation of amorphous cellulose. *Journal of Wood Chemistry and Technology*, **6**, 1–14.
66. Zhu, L., O'Dwyer, J.P., Chang, V.S. *et al.* (2008) Structural features affecting biomass enzymatic digestibility. *Bioresource Technology*, **99**, 3817–3828.
67. Pu, Y., Ziemer, C., and Ragauskas, A.J. (2006) CP/MAS ^{13}C NMR analysis of cellulase treated bleached softwood kraft pulp. *Carbohydrate Research*, **341**, 591–97.
68. Yamamoto, H. and Horii, F. (1993) CPMAS carbon-13 NMR analysis of the crystal transformation induced for Valonia cellulose by annealing at high temperatures. *Macromolecules*, **26**, 1313–1317.
69. Nishiyama, Y., Sugiyama, J., Chanzy, H., and Langan, P. (2003) Crystal structure and hydrogen bonding system in cellulose I_α from synchrotron x-ray and neutron fiber diffraction. *Journal of the American Chemical Society*, **125**, 14300–14306.
70. Larsson, P.T., Wickholm, K., and Iversen, T. (1997) A CP/MAS ^{13}C NMR investigation of molecular ordering in celluloses. *Carbohydrate Research*, **302**, 19–25.
71. Larsson, P.T., Hult, E.L., Wickholm, K. *et al.* (1999) CP/MAS ^{13}C-NMR spectroscopy applied to structure and interaction studies on cellulose I. *Solid State Nuclear Magnetic Resonance*, **15**, 31–40.
72. Larsson, P.T., Westermark, U., and Iversen, T. (1995) Determination of the cellulose Iα allomorph content in a tunicate cellulose by CP/MAS ^{13}C-NMR spectroscopy. *Carbohydrate Research*, **278**, 339–343.
73. Cateto, C., Hu, G., and Ragauskas, A.J. (2011) Enzymatic hydrolysis of organosolv Kanlow switchgrass and its impact on cellulose crystallinity and degree of polymerization. *Energy & Environmental Science*, **4**, 1516–1521.